CHALMERS
UNIVERSITY OF TECHNOLOGY

KU LEUVEN

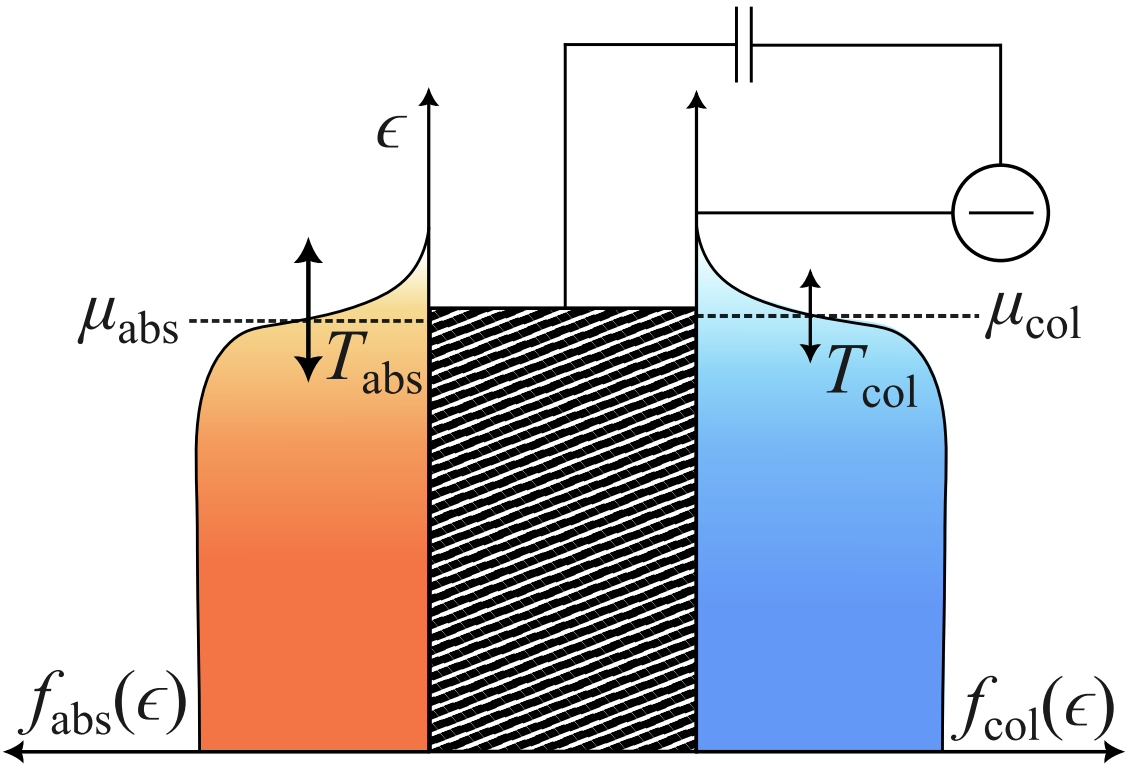

Feedback-driven optimization of hot-carrier solar cell

Thesis for the degree of Erasmus Mundus Master of Science
in Nanoscience and Nanotechnology

KRISHNA LYN DELIMA
Supervisor and Promoter: Prof. Janine Splettstößer
Daily Supervisor : Dr. Bruno Bertin-Johannet
Co-promoter: Prof. Bart Sorée

DEPARTMENT OF MICROTECHNOLOGY AND NANOSCIENCE (MC2)
CHALMERS UNIVERSITY OF TECHNOLOGY
Gothenburg, Sweden 2025
www.chalmers.se

THESIS FOR THE DEGREE OF
ERASMUS MUNDUS MASTER OF SCIENCE IN
NANOSCIENCE AND NANOTECHNOLOGY

Feedback-driven optimization of hot-carrier solar cell

KRISHNA LYN DELIMA

CHALMERS
UNIVERSITY OF TECHNOLOGY

Department of Microtechnology and Nanoscience (MC2)
Applied Quantum Physics Laboratory
Chalmers University of Technology
Gothenburg, Sweden 2025

Feedback-driven optimization of hot-carrier solar cell
KRISHNA LYN DELIMA

Thesis for the degree of Erasmus Mundus Master of Science in Nanoscience and Nanotechnology
This thesis was conducted in the framework of the Erasmus Mundus Master program in Nanoscience and Nanotechnology.

Promoter: Prof. Janine Splettstößer
Co-promoter: Prof. Bart Sorée
Daily Supervisor: Dr. Bruno Bertin-Johannet
External referee: Prof. Thilo Bauch

Applied Quantum Physics Laboratory
Department of Microtechnology and Nanoscience (MC2)
Chalmers University of Technology
SE-412 96 Gothenburg
Sweden

Faculty of Engineering Science
KU Leuven
3000 Leuven
Belgium

Cover: Energy diagram of a hot carrier solar cell with a feedback mechanism

Printed by Chalmers Reproservice
Gothenburg, Sweden 2025

Feedback-driven optimization of hot-carrier solar cell
Thesis for the degree of Erasmus Mundus Master of Science in Nanoscience and Nanotechnology
KRISHNA LYN DELIMA
Department of Microtechnology and Nanoscience
Chalmers University of Technology

Abstract

Solar cells convert energy absorbed from the sun into electrical power and they are therefore of high interest for green energy solutions. Ongoing research to improve solar cells deals with a broad range of aspects from improved light absorption to pushing the limits of efficiency searching for keys in materials research and device design.
Hot-carrier solar cells, which are at the focus of this thesis aim at improving the output power of a solar cell by exploiting the excess energy of the light-generated charge carriers, which is lost in fast relaxation processes in standard solar cells. The drawback of these hot-carrier solar cells is however that low-energy charge carriers are not exploited for power generation.
In this thesis, we propose and theoretically analyse a feedback mechanism to adapt the energy-filtering scheme for the extraction of hot carriers to the nonequilibrium conditions under which the solar cell is operated. This is done by coupling a quantum dot to the electron collector, which thereby measures the collector's potential. This quantum dot is furthermore capacitively coupled to the energy filter, so that it modifies its properties depending on the collector potential. We demonstrate that this feedback can improve the charging time, when the solar cell is used to charge a battery, and it can improve the power generated, when the solar cell is connected to a circuit with a load.
In this thesis we use a scattering matrix approach to model the solar cell operation. The load resistance or battery capacitance, as well as the filter properties enter the model through general variables, which could in the future be adapted to experimentally relevant conditions, in order to test the opportunities of this proposal for realistic devices.

Keywords: solar cells, hot carrier solar cell, quantum dot, quantum point contact, feedback optimization

Acknowledgements

First and foremost, I would like to thank my supervisors, Janine Splettstößer and Bruno Bertin-Johannet, for their unrelenting guidance and support throughout my internship. Janine has always provided such a welcoming atmosphere that drew me to continue working as her intern. She's like an endless trove of knowledge who's also so considerate in sharing her experiences. I am also truly grateful for Bruno's endless patience with me as I rummage through the world of thermodynamics. You have always provided steady support (especially when my codes stop working). I look forward to to working for both of you.
I am also thankful for this EMM-Nano program that has provided me opportunities I never would have imagined. Through this program, I've met life-long friends from different parts of the world and experienced things I could only dream of before. My friends, you know who you are, thanks for being my source of comfort and fun.
I am also truly grateful for my loving family. My siblings have been my source of happiness as long as I can remember. My grandpa, Tatay, I miss you so much. I wish you're still here with us so you can see what your unconditional love has done to my life. My Nanay who has always showered me with love and endless patience. The little girl you've been bringing to school everyday is now here. To my Mama, who raised us alone, I can never imagine how one can achieve as much as you have now. You always put us first before yourself. Now it's going to be my turn.
Lastly, but not the least, I want to thank my boyfriend, Felix, for always being there and for being my sanctuary ever since I met you 5 years ago.

Maupay na salamat!
Krishna

Contents

List of Figures

1
Introduction

1.1 Solar Cells

Since the Sun provides the Earth with a limitless supply of sunlight, converting solar energy to electrical power holds great promise. Harnessing the full potential of solar energy can eliminate the need to burn fossil fuels, which will in turn greatly decrease the amount of greenhouse gases that contribute to global warming and climate change [2].

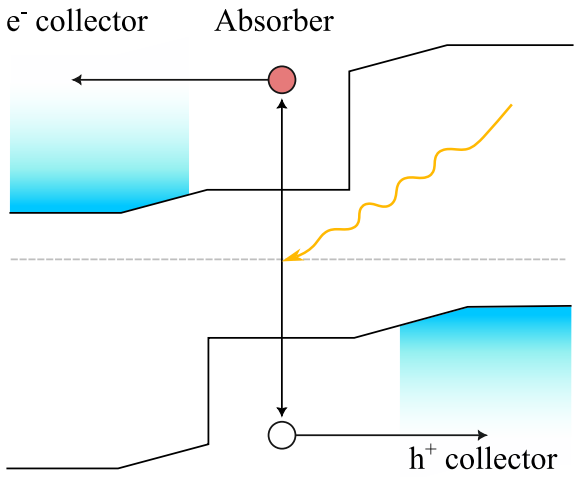

Figure 1.1: Schematic diagram of a solar cell When the absorber is irradiated by sunlight, an electron-hole pair is generated. Then, the pair separate and move towards their respective collectors. In standard solar cells, electrons and holes are transported to their collectors independently of their energy (above the bandgap). Figure adopted from Ref. [1]

Solar cells are devices capable of converting solar energy to electricity governed by the mechanism called *photovoltaic effect*, which was first observed by A.E. Becquerel in 1839. In an experiment involving metal electrodes in an electrolyte solution, he discovered that a small electric current was produced when illuminating certain materials [3]. This phenomenon wasn't fully explained until Albert Einstein proposed his *Photoelectric theory* in 1905. Using the ideas previously proposed by Planck, Einstein described that photons, if their energy is sufficiently large, can eject an electron from the surface of the metal—naming the phenomenon as the *photoelectric effect* [4].
The same phenomenon governs the workings of the solar cell. A standard solar

cell (Figure 1.1) is composed of electronic contacts, namely, an absorber and electron and hole collectors. When sunlight hits the absorber in the form of photons, electron-hole pairs are created. Due to the spatial asymmetry designed in the device and the effective potential difference between electrons and holes in the absorber, these photogenerated carriers separate and are extracted by their respective collectors inducing the current to flow through the load [4, 5]. Therefore, the electrical power generated by the solar cell is the product of the induced potential difference between absorber and collector and the generated current flowing through the load. Unfortunately, as effective as it may sound, there are various energy loss mechanisms at play that lower the efficiency of a conventional solar cell in reality, namely, carrier thermalization, relaxation, and recombination [6]. Carriers that carry a substantial amount of energy in excess of the bandgap are called *hot carriers*. In conventional solar cells, these hot carriers quickly lose a substantial part of their energy once these energy loss mechanisms take place [1, 6–8]. This energy is hence lost in standard solar cells.

1.2 Hot Carrier Solar Cells

In order to solve this challenge, the concept of *hot carrier solar cell* (HCSC) was proposed in 1982 by Ross and Nozik. It aims to extract these hot carriers before their excess energy dissipates as heat [7]. This device was set to push the maximum power conversion efficiency (PCE) of solar cells to 66% from the Shockley-Queisser limit of 30% [7, 9]. Since there has yet to be experimental proof of HCSC exceeding such limit, this concept is being rigorously studied due to its great potential.
The main goal of our HCSC is to extract these hot carriers before these energy loss mechanisms take place. To exploit this extra energy, energy filtering is explored which stems from an energy-dependent transmission between absorber and collectors [6, 9–12]. The filter, illustrated in Figure 1.1, selectively extracts hot carriers and thereby prevents backflow from the collectors [1]. Unfortunately, as a result, energy filtering also reduces the amount of carriers flowing towards the collector, having the downside to lower the current. Importantly, as a tradeoff, there can be a higher potential difference due to the blocked backflow from the collectors giving rise to higher power. The ideal filter height is, hence, determined from the tradeoff between reducing the current and increasing the potential.
In practical designs of HCSC, it's important to ensure that energies are indeed not lost. Initially, Ross and Nozik conceptualized HCSC as a "quantum-utilizing" device that allows hot carriers to equilibrate with each other instead of the environment to prevent energy loss [7]. More ways to delay the thermalization or carrier cooling were examined [9, 13, 14]. This thesis focuses on energy filtering to optimize extraction. Energy loss mechanisms are not studied here.
Even when we have successfully created an HCSC that exceeds the limits of efficiency of conventional solar cells, there are still various factors that we are not in control of that can significantly affect the performance of the solar cell. Primarily, no solar energy can be harvested at night. Also, within a single day, depending on the geographical location, the weather varies multiple times and this can limit the amount of sunlight that can be absorbed, and therefore, lowers the efficiency of the

cell. Thus, a filter height that adapts to varying illumination conditions would be highly beneficial.

1.3 Feedback Optimization

The main goal of this thesis is to propose a HCSC that can adapt to different nonequilibrium conditions arising from the amount of illumination and from the potential difference between absorber and collector (or across the load) this illumination entails.
When the weather is sunny, due to the increase in the temperature of the absorber, we would want a higher filter height to selectively extract carriers residing in the higher energy states. On the other hand, during a cloudy day, in response to the change in the distribution of the absorber, the filter height should ideally be lower to avoid blocking all carriers completely and still manage to extract charge carriers in the lower energy states (in comparison to the sunny case). Therefore, to optimize carrier extraction, it would be desirable for the filter height to autonomously adapt to changing weather conditions. We, therefore, propose a feedback mechanism where the energy filtering properties depend on the non-equilibrium conditions between the absorber and collectors.
After establishing a feedback mechanism, we explore the HCSC in two different ways: in storing the energy and in using the energy directly. The former involves treating the collector as a metallic island or "battery" that needs to be charged. The charge accumulated in the battery is characterized by a time-dependent chemical potential. On the other hand, in the latter, we add a load that turns current into power directly. In this case, the performance is characterized by the steady-state power output of the cell. In both setups, scattering theory is adopted to calculate the currents in our HCSC model [6].
To summarize, the goal of this thesis is to theoretically implement and optimize an autonomous feedback mechanism in a hot carrier solar cell device that adapts to varying illumination conditions whether it aims to charge a battery or to power a load.

1.4 Thesis Outline

After the general background and motivations have been laid out in this introductory chapter, chapter 2 follows by introducing the scattering theory that provides the mathematical framework to model the HCSC. Moreover, we explain how to model the feedback mechanism using the same formalism. Currents are defined separately for the cases with and without feedback. We provide comparisons of the power obtained from the solar-cell operations without feedback versus with feedback highlighting them throughout this study to assess the effectiveness of the feedback mechanism in place.
The next chapters present results of the aforementioned setups depending on how the HCSC is utilized. Chapter 3 shows how to optimize the steady-state power output being delivered to the load in a closed-circuit configuration. The best parameters

are numerically determined for both the cases with and without feedback. Then, their maximum power output is compared against a change in temperature (from sunny to cloudy).
In chapter 4, we examine the "battery" setup by looking into the evolution of the time-dependent chemical potential at varying filter heights in an open-circuit configuration and to investigate the impact of the feedback mechanism. Then, the charging time is set to add a physical constraint to the system. This chapter ends with providing the steps on how to build an optimized feedback-supported hot carrier solar cell for charging batteries. Finally, the conclusions are drawn in Chapter 5, supplied with ideas for further research.

2

Modeling the Solar Cell

2.1 Thermoelectric Model

To describe the physics behind the hot carrier solar cell, we focus on a simple model of a solar cell, which is basically the equivalent of a thermoelectric. The thermoelectric picture of a solar cell can be depicted in an energy diagram, see Fig. 2.1. The absorber and the collector are then characterized by occupation probabilities described by the Fermi-Dirac distribution at different temperature and electrochemical potentials:

$$f(\epsilon) = \frac{1}{1 + \exp[(\epsilon - \mu)/k_B T]} \tag{2.1}$$

where k_B is the Boltzmann constant[1].
In order to justify this model, two important steps or assumptions are taken. First, we have chosen to focus solely on the electron contribution in our figures and calculations for simplicity throughout this thesis. Indeed, Fig. 2.1 shown one single

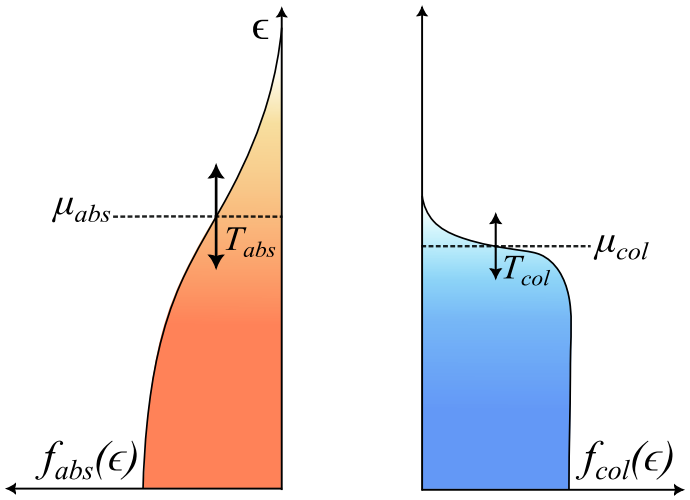

Figure 2.1: Solar cell before relaxation. Due to the high temperature in the absorber, the thermal distribution is spread out reaching higher energy states where these hot carriers reside.

collector for electrons only. The absorber potential is furthermore taken to correspond to the effective potential for electrons that would occur in a solar cell. The results for the power presented in this thesis hence correspond to the power obtained

[1]This thesis follows the natural units system for simplification. Hence, $\hbar, k_B = 1$.

from the electronic contribution and the (analogous) hole contribution would need to be added to obtain the full power. Second, in our hot carrier solar cell model, we assume that carriers have thermalized but haven't relaxed to match the ambient temperature of the collector, T_{col}. This means that the distribution in the absorber exhibits "hot" thermal distribution compared to the "cold" thermal distribution of the collector as illustrated in Figure 2.1.
Non-thermal distributions in the collector have been considered in Refs. [6, 15].
Using this thermoelectric picture, we now model the solar cell, by a two-terminal system given a hot and cold distribution connected to each other by a coherent conductor with energy-dependent transmission. Using this model, we study two

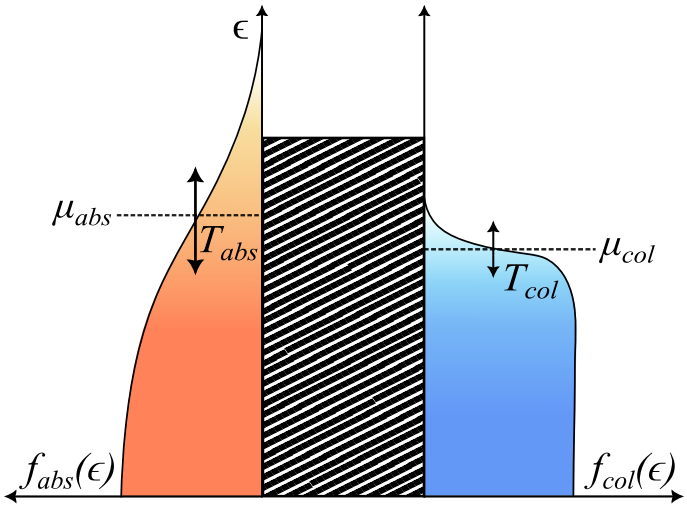

Figure 2.2: Hot carrier solar cell with an energy filter, in the absence of any feedback mechanism.

operational modes on how the hot carrier solar cell could be employed. First, we study a closed circuit where a load connects the two contacts with a fixed resistance. Here, the maximum power output is examined as follows:

$$P = IV = V^2/R. \tag{2.2}$$

The other setup involves an open circuit where the temperature difference between two contacts creates a thermovoltage. Here, the time-dependent chemical potential is looked into to describe charge accumulation in the battery. We refer to this as "charging the battery" and this is discussed in chapter 4. In both cases, defining the current is crucial as we need this to calculate for the time-dependent chemical potential for the battery setup, and for obtaining the maximum power in the load setup.

2.2 Scattering Theory

To calculate generated current, we employ the scattering theory. This theory set forth by Landauer and Büttiker [16, 17] has been widely-used as a theoretical formalism to describe electron transport in mesoscopic systems [18]. In this approach,

carrier interactions are neglected or treated at a mean-field level [6, 19]. Figure 2.2 illustrates the hot-carrier solar-cell model. The current from the absorber entering the collector is given by

$$I = \frac{e}{2\pi} \int_0^\infty d\epsilon \; D(\epsilon) \, [f_{abs}(\epsilon) - f_{col}(\epsilon)]. \tag{2.3}$$

Here, f_{abs} and f_{col} are the Fermi-Dirac functions representing the distribution in the absorber

$$f_{abs}(\epsilon) = \frac{1}{1 + \exp[(\epsilon - \mu_{abs})/T_{abs}]} \tag{2.4}$$

and collector, respectively

$$f_{col}(\epsilon) = \frac{1}{1 + \exp[(\epsilon - \mu_{col})/T_{col}]}. \tag{2.5}$$

Note that we consider μ_{abs} to be zero to serve as reference here, $\mu_{abs} \equiv 0$ and μ_{col} changes depending the operation of the solar-cell circuit. The temperatures of the two contacts are chosen to represent the thermal distribution of carriers created at the temperature of the sun, $T_{abs} \simeq 6000\,K$ in the absorber. On the other hand, T_{col} stands for the ambient temperature of the environment around $300\,K$. We will in this report refer to situations where the temperatures are chosen as $T_{abs} = 20T_{col}$ as “sunny" and we will furthermore chose a different condition with $T_{abs} = 10T_{col}$, which we will refer to as “cloudy".
The filter is represented by $D(\epsilon)$, which is the transmission probability modeled as a step function:

$$D(\epsilon) = \begin{cases} 1 & \text{if } \epsilon > \epsilon_1 \\ 0 & \text{if } \epsilon < \epsilon_1. \end{cases} \tag{2.6}$$

Here, ϵ_1 is the filter height, see Fig. 2.2. In various experiments, this step-function transmission is usually implemented by using a quantum point contact (QPC) [6, 20–22]. As seen in Figure 2.3, in a QPC the width of the constriction can be engineered by the application of gate voltages to only allow carriers of certain energies to pass through. When connected to the absorber and collector contacts it hence effectively works as a filter. Similar transmission probabilities to the one given in

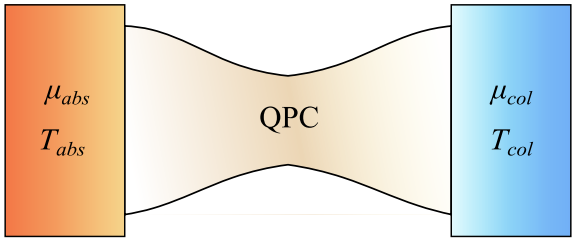

Figure 2.3: Quantum point contact (QPC) used as an energy filter in the hot carrier solar cell.

Eq. 2.6 have been realized in experiments by bandgap engineering in semiconductor heterostructures [23, 24].
After establishing the formalism used to describe the currents in the hot carrier solar cell in the absence of feedback, we now examine the relationship of these parameters with the interest of maximizing power output.

2.3 Power generation in the absence of a feedback

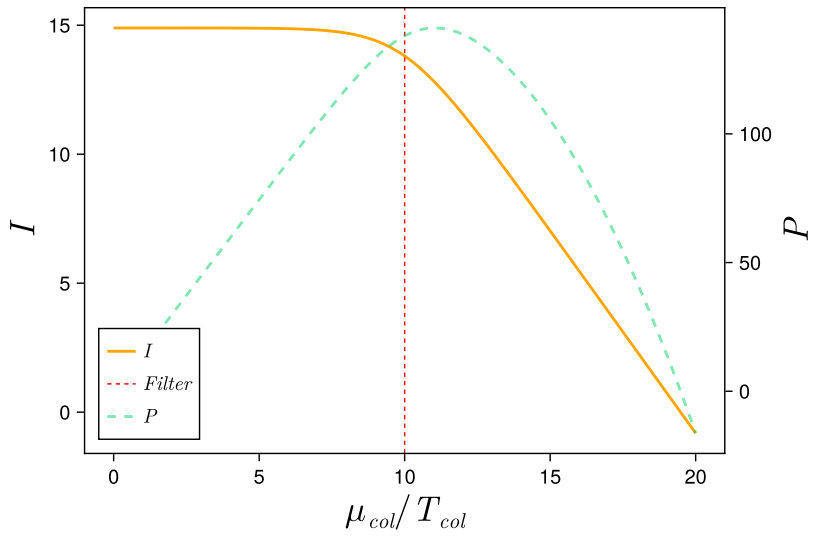

Figure 2.4: The current and power n arbitrary units as a function of chemical potential at $T_{abs} = 20\,T_{col}$.

We start by presenting how the power and current generated by a temperature difference in the system introduced above behaves. As a first simple step, we here assume that the potential difference between collector and absorber is given. Figure 2.4 shows the current and power as a function of this electrochemical potential μ_{col}. This plot shows what happens as the current flows toward the collector at filter height $\epsilon_1 = 10\,T_{col}$ and at absorber temperature $T_{abs} = 20\,T_{col}$.

As observed, the current has a plateau value depending on the temperature difference. It eventually goes to zero since the incoming current (absorber to the collector) is counteracted by the current backflow due to the increase in μ_{col}/T_{col} (collector to absorber) until they cancel each other out and the current vanishes. As expected, the current starts decreasing around the set filter height of $10\,T_{col}$. On the other hand, an initial steady increase has been observed in power due to the increasing chemical potential, μ_{col}/T_{col}. Then, the maximum power is reached above the filter height—again depending on the temperature difference between absorber and collector. This signifies the previously mentioned tradeoff of a reduced current and a higher potential difference that generates higher power. As said, balancing these two parameters would give us the ideal filter height.

It becomes clear here that an important parameter to consider when it comes to power generation is the temperature difference. As previously discussed, the illumination condition alters the temperature difference, which in turn causes nonequilibrium conditons that greatly influence the power output. Hence, a hot carrier solar cell that adapts to these changing weather conditions can greatly optimize power generation or charge accumulation in the "battery".

2.4 Feedback Mechanism

As previously mentioned, the amount of solar energy available can still vary during the day. Since sufficient sunlight is needed for solar cell, various factors such as clouds blocking the sun or a sudden rain shower can alter their efficiency. Hence, it

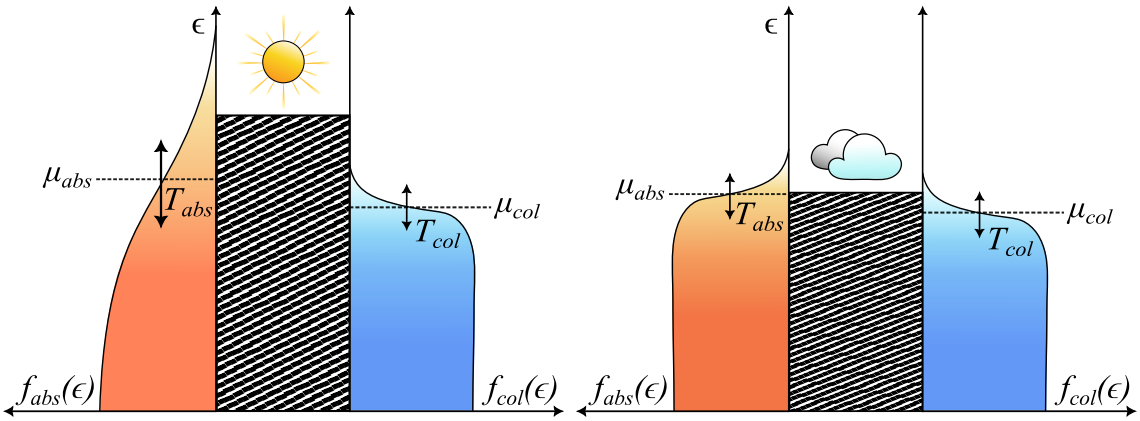

(a) Sunny case **(b)** Cloudy case

Figure 2.5: Ideal filter heights for different illumination conditions.

would be promising to create a hot carrier solar cell device that can adapt to different illumination conditions. As illustrated in Figure 2.5, when the weather is sunny, due to the increase in the temperature of the absorber, we would want a higher filter height to selectively extract carriers residing in the higher energy states. On the other hand, during a cloudy day, in response to the change in the distribution of the absorber, the filter height should ideally be lower to avoid blocking all carriers completely and still manage to extract hot carriers in the lower energy states (in comparison to the sunny case). Therefore, to optimize carrier extraction, it would be desirable for the filter height to autonomously adapt to changing weather conditions. The change of the output power with the filter hight depending on the temperature difference will be discussed in detail in the following two results chapters. Adjusting

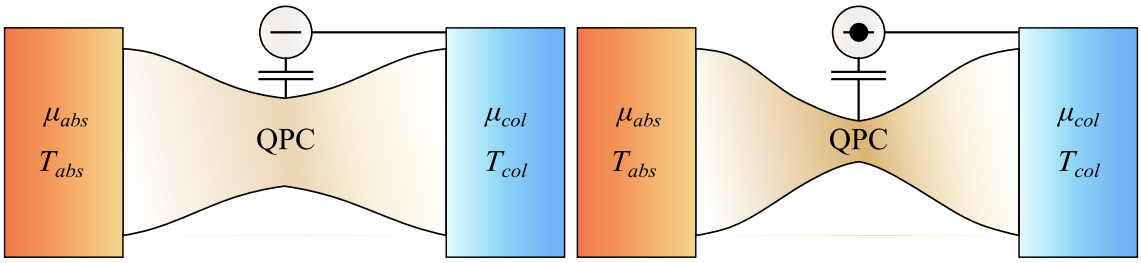

(a) Empty quantum dot **(b)** Filled quantum dot

Figure 2.6: Schematic diagram of the hot carrier solar cell with a feedback mechanism consisting of a quantum dot capacitively coupled to the QPC and tunnel coupled to the collector. When the quantum dot is filled, the QPC responds by a narrower constriction.

the parameters to the nonequilibrium conditions, is made possible by implementing a feedback mechanism.
In our hot carrier solar cell model, a quantum dot is added that is capacitively coupled to the QPC (filter) and tunnel coupled to the collector as depicted in Figure 2.6. This system was adopted from Ref. [25] where the quantum dot and QPC pairing was used in their device designed to operate as a noninvasive thermometer. In our model, the state—namely the occupation probability—of the quantum dot depends on the distribution in the collector and thereby measures it. At the same time, the quantum dot is capacitively coupled to the QPC (with interaction energy U) and the dot charge and exerts a potential on the QPC. This leads to a feedback mechanism since the QPC responds to the occupation of the dot. In Figure 2.6, this

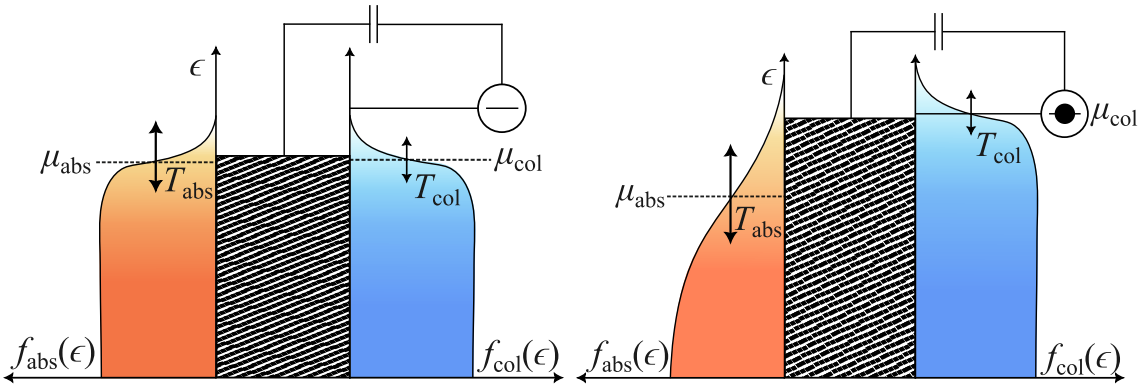

(a) Empty quantum dot **(b)** Filled quantum dot

Figure 2.7: Energy landscape of the hot carrier solar cell with a feedback mechanism. (a) When the potential in the collector is below the energy level of the dot, then the dot remains empty. (b) When the temperature of the absorber increases, more carriers flow towards the collector. Eventually, the potential in the collector increases and the dot gets filled. Since the QPC is sensitive to the population in the dot, this effectively increases the filter height.

is shown by a narrowing of the constriction of the QPC when the dot is occupied. Figure 2.7 describes how the feedback mechanism works by employing a sketch of the modified energy landscape depending on the dot occupation (which in turn depends on the collector potential). When it's cloudy, little current is induced between the absorber and collector and the distribution in the collector is not high enough to occupy the quantum dot. However, once it's sunny and the absorber receives more sunlight, the temperature of the absorber increases and more carriers are induced to flow towards the collector. Eventually, the potential in the collector increases to the point that the quantum dot gets filled and the QPC responds by increasing its energy, resulting in a higher filter height. Due to the increase in energy, the QPC should have a narrower constriction as shown in Figure 2.6b. In reverse, when the sun is suddenly blocked by some clouds, the quantum dot becomes empty and the QPC responds by lowering its energy. This interaction consists the feedback mechanism designed to respond to the varying amount of sunlight the absorber receives.
For the hot carrier solar cell with a feedback mechanism (Figure 2.7), the current is

defined below:

$$I = \frac{e}{2\pi} \int_0^\infty d\epsilon \; D_F(\epsilon) \left[f_{abs}(\epsilon) - f_{col}(\epsilon) \right] \tag{2.7}$$

where

$$D_F(\epsilon) = \begin{cases} 1 & \text{if } \epsilon > \epsilon_1 + \mathrm{U} f_{col}(\epsilon_{dot}) \\ 0 & \text{if } \epsilon < \epsilon_1 + \mathrm{U} f_{col}(\epsilon_{dot}) \end{cases} \tag{2.8}$$

This time, the energy-dependent transmission probability have incorporated the coupling parameter, U, and the level of quantum dot with respect to the distribution in the collector, $f_{col}(\epsilon_{dot})$. The coupling parameter is equivalent to

$$U = \frac{e^2}{C} \tag{2.9}$$

where C is the capacitance between quantum dot and QPC [25]. In this way, when the μ_{col} reaches the height of the ϵ_{dot}, the filter height is set to increase in energy, and this increase depends on the coupling parameter, U.
Throughout this thesis, comparisons between a solar cell with and without feedback are done to test the effectiveness of the feedback mechanism in place.

3

Generating a current across a load

The first configuration we study, presented in this section, is a closed-circuit configuration, where the solar cell is used to provide power directly to an electric device. This means that we are now studying the *steady-state* current in a closed-circuit configuration. The "device" is modeled by a load with resistance R, through which the thermo-current I flows, induced by the temperature difference between absorber and resistor which results from the light illumination. The current flowing through the load generates a power

$$P = RI^2. \tag{3.1}$$

We are now interested in obtaining the maximum power output in this closed-circuit configuration under steady-state operation. It is helpful for further calculation to express the power in terms of the voltage (or the potential drop) that arises due to the current flow across the load. To calculate for the power, we first apply Ohm's law,

$$V = IR, \tag{3.2}$$

to redefine it in terms of voltage, V,

$$P = V^2/R. \tag{3.3}$$

The voltage is then determined by finding the chemical potential, μ_{col}, by using the relation shown below

$$\mu_{col} = eV \Rightarrow V = \frac{\mu_{col}}{e}. \tag{3.4}$$

Hence, the calculated power becomes

$$P = \frac{\mu_{col}^2}{eR}. \tag{3.5}$$

The important next step is now to obtain the steady-state potential across the load, which is given by μ_{col}. Applying Ohm's law once again and using the expression for the current from the absorber to the collector discussed in eq. (2.3), we find the μ_{col}, shown below:

$$\mu_{col} = eR\, I(\mu_{col}) = \frac{e^2 R}{2\pi} \int_0^\infty d\epsilon\; D(\epsilon)\,[f_{abs}(\epsilon) - f_{col}(\epsilon)] \tag{3.6}$$

Here, $D(\epsilon)$ is the energy-dependent transmission probability described in eq. (2.6), which has step-shape where ϵ_1 is the height of the energy filter that we are using to extract the hot carriers from the absorber. Upon evaluation, the eq. (3.6) becomes

$$\mu_{col} = \frac{e^2 R}{2\pi} \left\{ T_{abs} \ln\!\left[1 + \exp\!\left(\frac{-\epsilon_1}{T_{abs}}\right)\right] - T_{col} \ln\!\left[1 + \exp\!\left(\frac{\mu_{col} - \epsilon_1}{T_{col}}\right)\right] \right\}. \tag{3.7}$$

When the feedback is added, μ_{col} is determined using:

$$\mu_{col} = \frac{e^2 R}{2\pi} \int_0^\infty d\epsilon \; D_F(\epsilon) \left[f_{abs}(\epsilon) - f_{col}(\epsilon) \right] \tag{3.8}$$

where D_F is the transmission probability that incorporates the feedback described in eq. (2.8). Upon evaluation, the eq. (3.8) becomes

$$\begin{aligned} \mu_{col} = \frac{e^2 R}{2\pi} \Bigg\{ & T_{abs} \ln \left[1 + \exp\left(\frac{-\epsilon_1 - \mathrm{U} f_{col}(\epsilon_{dot}).}{T_{abs}} \right) \right] \\ & - T_{col} \ln \left[1 + \exp\left(\frac{\mu_{col} - \mathrm{U} f_{col}(\epsilon_{dot}).}{T_{col}} \right) \right] \Bigg\} \end{aligned} \tag{3.9}$$

Here, U is the coupling parameter and ϵ_{dot} represents the energy-level position of the quantum dot that is used for measurement of the nonequilibrium condition and feedback. The expressions in Eq. (3.7) and (3.9) are self-consistent equations for the potential difference, which hence need to be solved numerically. In the following sections, we present results obtained numerically through *NonlinearSolve.jl* in Julia [26].
Using this μ_{col}, we calculate the generated power across the load in different parameter regimes—with and without feedback. The maximum power that can be obtained from a single-channel quantum conductor subject to a temperature difference, as studied here, is given by the power bound established by Whitney [27]. We will plot the calculated power values either in units of T_{col}^2/h or compared to this quantum upper bound of power P_W such as

$$\frac{P}{P_W} = \frac{P}{0.0321 \frac{\pi}{h} (T_{abs} - T_{col})^2}. \tag{3.10}$$

In the following, we analyze the power delivered to the load and examine how optimizing the parameters such as the resistance R of the load and ϵ_1 can improve performance.

3.1 Optimizing power through load

The first task is to analyze how the power that is produced when a current is generated depends on the nonequilibrium conditions and on the tunable parameters. We therefore first examine the power across different filter heights at varying resistances. In Figure 3.1, we plot the power as a function of the filter height for different values of the load resistance at a temperature ratio $T_{abs} = 10\, T_{col}$. We recall that this is the temperature setting that we refer to as “cloudy".
We observe that the power reaches a maximum at a given value of the filter height. The value of this maximum and its position change with the resistance of the connected load. The highest maximum power is obtained at $R = 20\, h/e^2$ among the range of resistances given.
Henceforth, to find the optimal power generation, we need to optimize the filter height and the resistance of the load. This power that we described is a product of

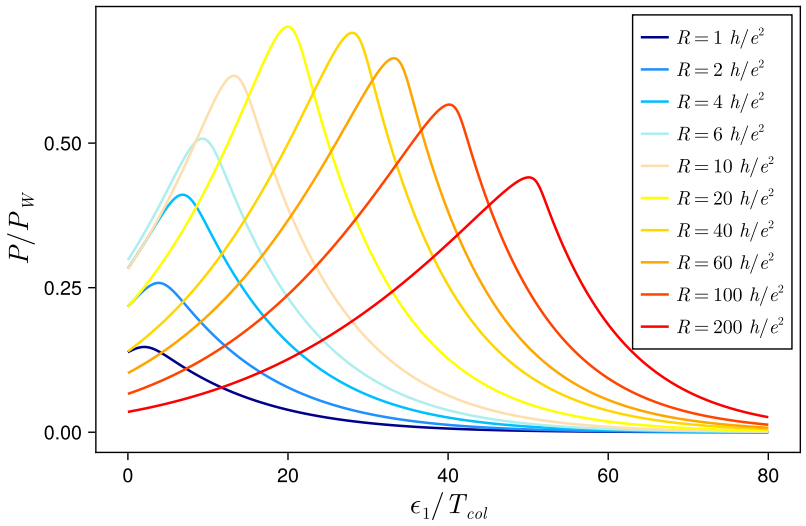

Figure 3.1: Power as a function of the filter height ϵ_1 for different resistances. Maximum power is reached at a certain filter height, where maximum value and position change with the load resistance.

current and voltage,which are proportional to each other, as can be seen by their linear relationship according to Ohm's law, as expressed in eq. (3.2). Thus, we plot μ as a function of ϵ_1 in Figure 3.2 at $T_{abs} = 10\,T_{col}$ and found that the induced potential has a maximum at a finite filter height, namely when the filter is placed approximately $10\,T_{col}$ above the potential of the absorber. Here, we observe the importance of setting a proper filter height to maximize the potential difference that leads to an optimized power output.

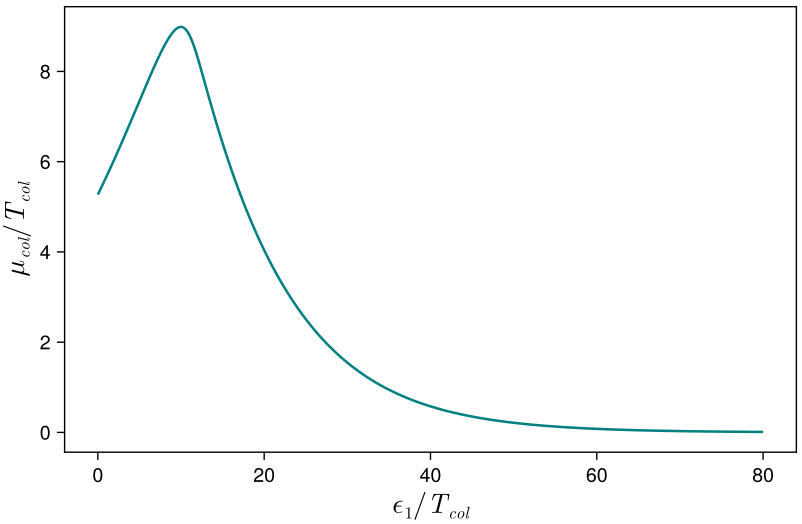

Figure 3.2: Chemical potential μ as a function of ϵ_1. The maximum is reached at approximately $\epsilon_1 = 10\,T_{col}$ at $T_{abs} = 10\,T_{col}$.

As a next step, we optimize the power over both the resistance of the load and over the filter height.
We plot the power optimized over filter height as a function of the resistance of the

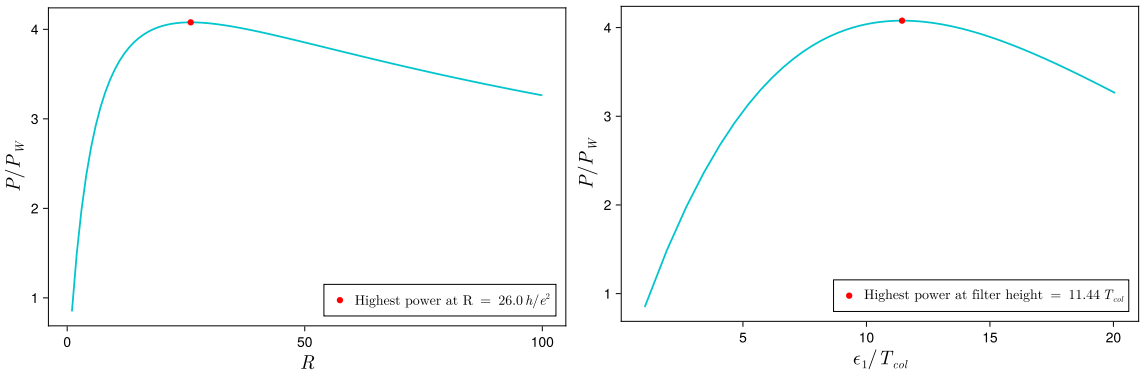

(a) Ideal resistance value **(b)** Ideal filter height

Figure 3.3: Optimizations on power to find the optimal R and ϵ_1.

load in Figure 3.3a. We find that it reaches a maximum at a value of $R = 26\,h/e^2$. Analogously, in Figure 3.3b, we show the power optimized over R plotted as a function of ϵ_1. Similarly, a maximum is reached for ϵ_1 at $22.88\,T_{col}$. These two maxima correspond to each other. The two different curves presented in 3.3a and 3.3b show how this maximum value is reached. This method of finding optimized parameters is applicable to a scenario with no feedback. However, also here, we are interested in finding out how the performance can be further increased by adapting the filtering mechanism to the nonequilibrium conditions.

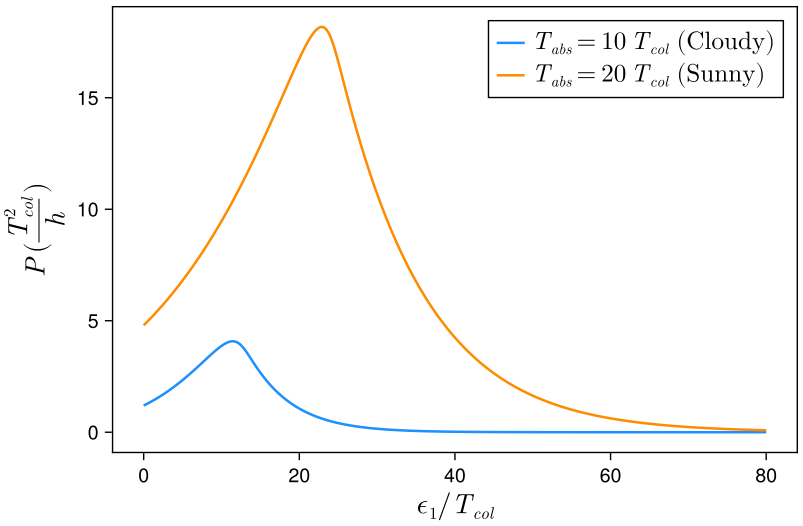

Figure 3.4: Power over increasing ϵ_1. This demonstrates that the ideal filter height to reach the maximum power increases with temperature difference.

In order to analyze how the power depends on the illumination condition, we now plot power as a function of ϵ_1 for the two temperature ratios,which we refer to as cloudy ($T_{abs} = 10\,T_{col}$) and sunny ($T_{abs} = 20\,T_{col}$), in Figure 3.4. As expected, the higher temperature difference generated a higher power output. We furthermore observe that the temperature difference influences the required filter height to reach the maximum power. In particular, we see that the ideal filter height increases with temperature difference. Therefore, in the next section, we implement a feedback

mechanism to change the parameters of the setup according to the temperature difference.

3.2 Feedback optimization of the power

In this section, we use feedback to optimize the solar cell depending on the illumination conditions. We here assume for a first simplified approach that the solar cell always operates under either one fixed cloudy or one fixed sunny condition and disregard any intermediate temperature difference. The feedback mechanism based on the quantum dot described in Chapter 2 does not impact the resistance. Therefore, in order to build the feedback setup, we choose a fixed value of R given by the optimized resistance found in the previous section in the cloudy situation, i.e., $R = 26\,h/e^2$.
From Fig. 3.4, it is clear that an ideal feedback mechanism would "choose" to switch between the two filter heights that yield the maximum power values for cloudy and sunny conditions. We now analyze how this can be done based on a measurement of the potential build-up. In Figure 3.5, the power and μ_{col} are plotted as a function of ϵ_1 in both sunny and cloudy situations, for $R = 26\,h/e^2$. As already observed

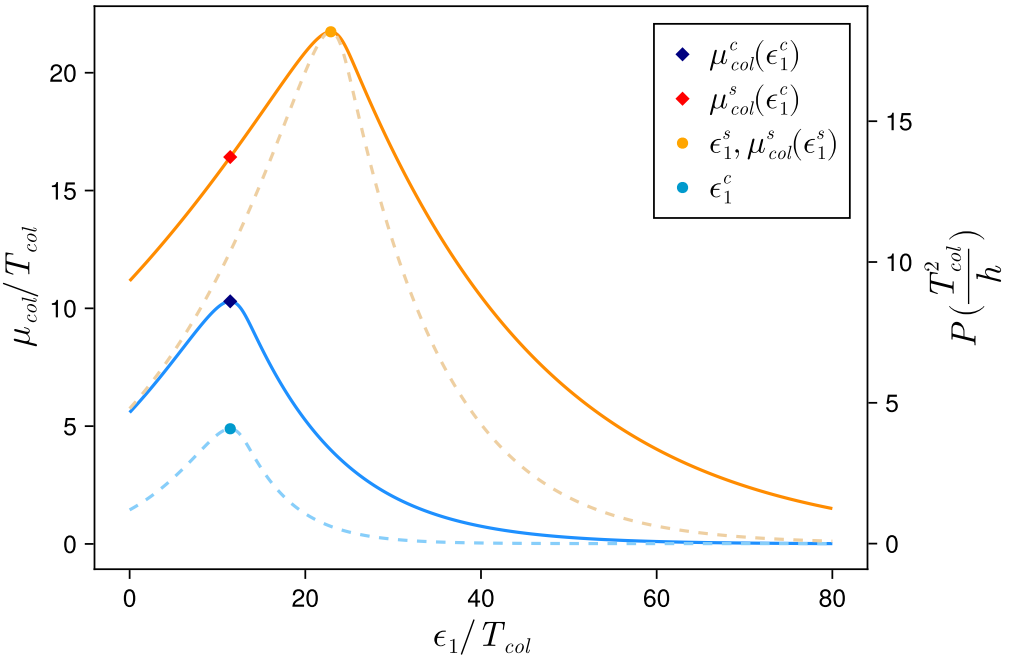

Figure 3.5: Chemical potential (solid lines) and power (dashed lines) as a function of filter height for $T_{abs} = 20\,T_{col}$ (sunny, orange line) and $T_{abs} = 10\,T_{col}$ (cloudy, blue line). Best filter heights per temperature difference were obtained: ϵ^s_1 for the sunny condition (orange) at $T_{abs} = 20\,T_{col}$ and ϵ^c_1 for the cloudy condition (blue) at $T_{abs} = 10\,T_{col}$. The maximum chemical potentials are also acquired: $\mu^c_{col}(\epsilon^c_1)$ for the cloudy condition and $\mu^s_{col}(\epsilon^s_1)$ for the sunny condition. A vital point in the chemical potential for the sunny condition, $\mu^s_{col}(\epsilon^c_1)$, is taken based on the best filter height for a cloudy condition. All these parameters are useful for optimizing the hot carrier solar cell using a feedback.

in the previous section, the maximum power is reached at specific filter heights depending on the temperature difference. We now start by finding the best filter height when $T_{abs} = 20\,T_{col}$. We obtain a higher ideal filter height, $\epsilon_1 = 22.88\,T_{col}$, for the sunny condition and we refer to this value as ϵ_1^s. By contrast, ϵ_1^c pertains to the ideal filter height for the cloudy condition. Ideally, when the temperature increases from $T_{abs} = 10\,T_{col}$ to $20\,T_{col}$, we would want the filter height to lift from ϵ_1^c to ϵ_1^s. Hence, this change in height, as mentioned in chapter 2, needs to be governed by the coupling parameter, U, which is then chosen as

$$U = \epsilon_1^s - \epsilon_1^c. \tag{3.11}$$

This is the shift that should be reached from the feedback. Now, to initiate this change in filter height, the quantum dot is used to detect the distribution in the collector, and once it's occupied, it effectively switches the filter height from ϵ_1^c to ϵ_1^s, if the quantum dot is empty under cloudy conditions and fully occupied under sunny conditions (ideal measurement). Hence, we now need to find the energy at which to place the quantum-dot energy level such that it can reliably distinguish between the two illumination conditions. We argue that the ideal quantum dot energy-level position is

$$\epsilon_{dot} = \frac{\mu_{col}^s(\epsilon_1^c) + \mu_{col}^c(\epsilon_1^c)}{2}. \tag{3.12}$$

In the following, we explain, using Fig. 3.5, how this value is obtained. The parameter $\mu_{col}^c(\epsilon_1^c)$ is the maximum chemical potential in the cloudy condition while $\mu_{col}^s(\epsilon_1^c)$ is the potential in the sunny condition when the filter height is at ϵ_1^c. Placing the dot between these chemical potential levels allows the dot to respond to the non-equilibrium conditions in the collector brought by temperature difference changes. Indeed, in this case, the dot would be empty in cloudy conditions, so the filter height would be ϵ_1^c, and filled in sunny conditions with a filter height modified by feedback such that it reaches $\epsilon_1^c + \mathrm{U} = \epsilon_1^s$. In this way, the device is optimized both in sunny and cloudy conditions. Note that the eqs. (3.11) and (3.12) are obviously valid independent of the direction in which the change in temperature difference between $T_{abs} = 20\,T_{col}$ and $10\,T_{col}$ occurs.

To illustrate this feedback mechanism, a simple scenario in which the weather changes from cloudy to sunny and back to cloudy, is proposed. The temperature T_{abs} starts at $T = 10\,T_{col}$ at $t = 0$, then at a certain time t_1, the temperature is, for simplicity, assumed to instantaneously increase to $T_{abs} = 20\,T_{col}$, and to finally decrease to $T = 10\,T_{col}$ at time t_2.

The power obtained with the feedback mechanism, P_F, in this scenario is plotted as it changes with the different settings in Figure 3.6. We also plot the power obtained without the feedback for ϵ_1^s, P_s (beige) and for ϵ_1^c, P_c (skyblue). We can see how the feedback setup showed significant adaptability since it effectively responded to the changing T_{abs}. As expected, P_s and P_c, which are optimized for sunny and cloudy conditions, respectively, are not comparably as effective in adapting to the other condition.

Thus, we successfully demonstrated how the feedback improves the adaptability of the hot carrier solar cells to two distinct temperature difference. However, more research is needed to improve the power generation for this closed circuit configuration.

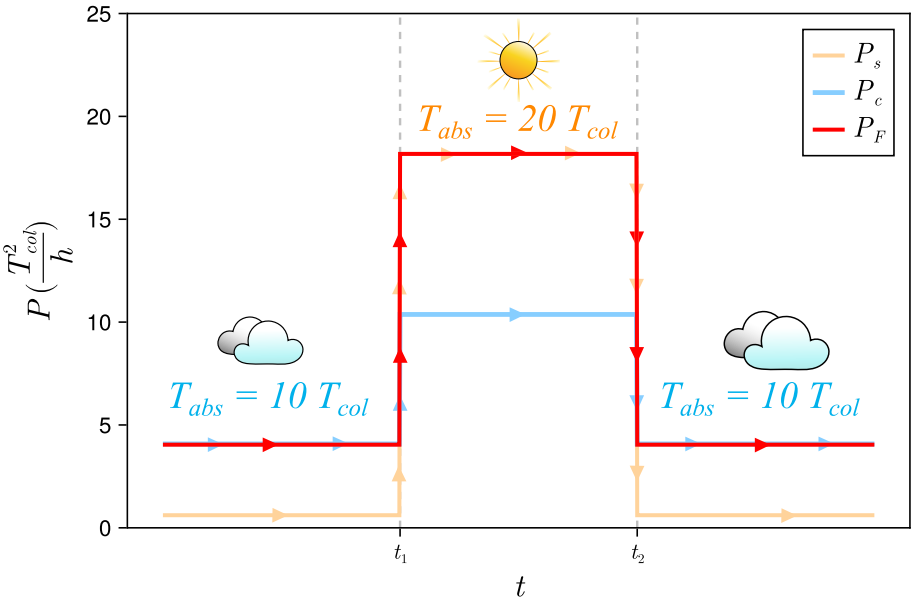

Figure 3.6: Plot of the power vs time with shifting temperature at t1 and t2 from cloudy to sunny then sunny to cloudy. Comparison of powers of the no feedback case (P_s, P_c) but optimized to their corresponding temperature ratios and the power of the with feedback case with optimal parameters (P_F).

Here, we have chosen an intuitive way to find the best conditions for feedback. As next steps, we will also analyze to which settings the required values of U would correspond in realistic experimental settings. And we will also analyze how deviations from the ideal measurements would impact the performance. Furthermore, a general numerical optimization procedure is planned for general temperature differences for this steady-state closed-circuit configuration with a load.

4

Charging the "battery"

As opposed to the previous section, where the solar cell is directly linked to a load and power output was optimized, presented in this chapter is an open-circuit configuration, where the collector is a metallic island acting like a battery that gets charged when the solar cell is illuminated. Due to the temperature difference between the absorber and the collector, a current is flowing through the junction, creating a charge buildup in the collector. This charge buildup is characterized by a chemical potential μ. The steady state is reached when the chemical potential is high enough so that no current is flowing (namely the particle flow induced by the temperature difference is canceled by the backflow from the collector to the absorber). The potential difference that arises in the steady-state limit, is referred to as the *stopping voltage*. It is related to the maximum charge that the battery can be filled with when connected to the solar cell irradiated by light. This charge of the battery is connected to the potential buildup via the relation:

$$CV = Q \tag{4.1}$$

for the charge on a capacitor plate. Indeed, the system behaves in many ways as a capacitor: the time it takes to reach the steady state or to charge the "battery" is the RC-time of the corresponding capacitor. The RC time of quantum capacitors has been studied in Refs. [28, 29].
Since the time it takes to reach the stopping voltage can be very long depending on the transmission properties of the conductor (relating to the resistance R) and on the capacitance (quantum and geometrical capacitance $C = C_g + C_\mu$) of the circuit element to be charged, it can be of practical relevance to also study the stopping voltage that can be reached in a given charging time. Thus, in this section, we analyze both the stopping voltage as well as the potential buildup in a given charging time, as a function of the (light-induced) non equilibrium properties and the filter properties.
The potential buildup in the collector of the HCSC is derived as follows. Considering the collector as a battery described by a density of state $\nu(\epsilon)$

$$q = eN = e \int d\epsilon\, \nu(\epsilon)\, f_{col}(\epsilon) \tag{4.2}$$

where e is the charge of the electron, $\nu(\epsilon)$, and f_{col} is the Fermi function of the collector. The current as a function of chemical potential $I(\mu)$ is then found by writing $I = \frac{dq}{dt}$:

$$I(\mu) = \frac{dq}{d\mu} \cdot \frac{d\mu}{dt} = e \int d\epsilon\, \nu(\epsilon)\, \frac{df_{col}(\mu)}{d\mu} \cdot \frac{d\mu}{dt} \tag{4.3}$$

We are interested in obtaining the $d\mu/dt$ to obtain the potential buildup as a function of time. Thus, we first write $dq/d\mu$, which, after expanding $df_{col}(\mu)/d\mu$, looks like:

$$\frac{dq}{d\mu} = e\int_{\epsilon_1}^{\infty} d\epsilon\, \nu(\epsilon)\, \frac{\exp\left(\frac{\epsilon-\mu_{col}}{T_{col}}\right)/T_{col}}{\left(1+\exp\left(\frac{\epsilon-\mu_{col}}{T_{col}}\right)\right)^2}. \tag{4.4}$$

Then, in the simplest case, we assume constant density of states in the island $\nu(\epsilon) = 2\pi A\nu^0$ (where A is the area of the collector), taking it out of the integral we get:

$$\frac{dq}{d\mu} = e\,2\pi A\nu^0 \int_{\epsilon_1}^{\infty} d\epsilon\, \frac{\exp\left(\frac{\epsilon-\mu_{col}}{T_{col}}\right)/T_{col}}{\left(1+\exp\left(\frac{\epsilon-\mu_{col}}{T_{col}}\right)\right)^2}. \tag{4.5}$$

Upon the evaluation of this integral, we arrive at the final form of $dq/d\mu$:

$$\frac{dq}{du} = e2\pi A\nu^0 \left[1+\exp\left(-\frac{\mu_{col}}{T_{col}}\right)\right]^{-1} \tag{4.6}$$

Then, by isolating $d\mu/dt$ in Eq. (4.3) and by using the equation for the current (in the no feedback case) Eq. (2.3), we find the potential build up as:

$$\begin{aligned}\frac{d\mu}{dt} = \frac{1}{2\pi A\nu^0}\left[1+\exp\left(-\frac{\mu(t)}{T_{col}}\right)\right] \times \Bigg\{ T_{abs}\ln\left[1+\exp\left(-\frac{\epsilon_1}{T_{abs}}\right)\right] \\ - T_{col}\ln\left[1+\exp\left(\frac{\mu(t)-\epsilon_1}{T_{col}}\right)\right]\Bigg\}.\end{aligned} \tag{4.7}$$

The differential equation (4.7) above was numerically solved using the *Differen-*

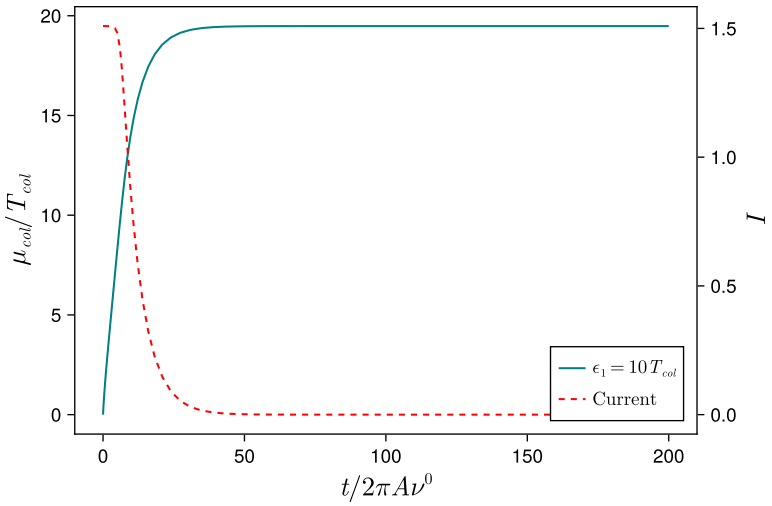

Figure 4.1: Chemical potential as a function of time with the set filter height at $\epsilon_1 = 10\,T_{col}$. We observe that the potential increases with time while the current decreases with time. The maximum potential where the current gets to zero is the stopping voltage.

tialEquations.jl package in Julia [30].

In Figure 4.1, we plot the behavior of μ and of the current in the collector as a function of time where the filter height is at $\epsilon_1 = 10\,T_{col}$ within a time span of $t = 0 - 200 \times 2\pi A\nu^0$. We see that the potential increases and that the current decreases with time. The chemical potential, μ_{col}/T_{col}, plateaus at a certain maximum, and at the same time the current completely vanishes. The maximum potential (at which the current vanishes) is the stopping voltage, here $\mu_{col} \approx 19\,T_{\text{col}}$. The goal in this battery setup is to achieve a high stopping voltage. Hence, we will look into the ideal filter height that is required in order to obtain the highest stopping voltage possible.

4.1 Stopping Voltage

Focusing on the infinite time limit, Figure 4.2 shows the stopping voltage as a func-

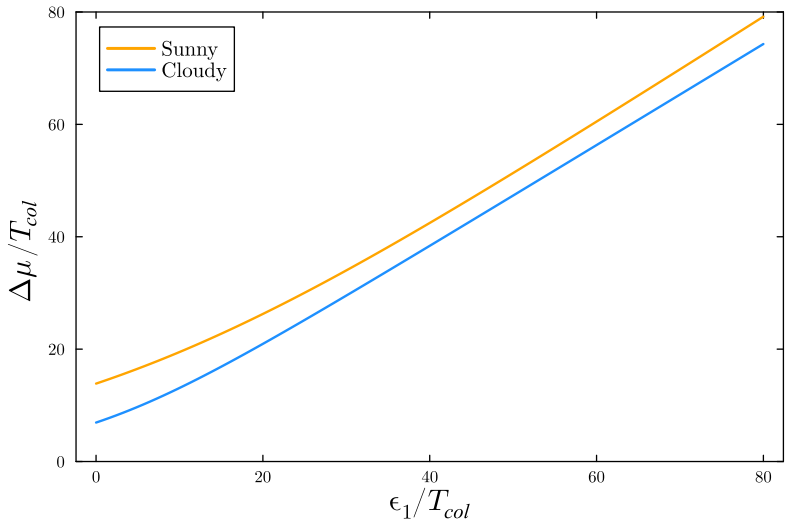

Figure 4.2: Stopping voltage as a function of filter height for two temperature differences: sunny ($T_{abs} = 20\,T_{col}$) and cloudy ($T_{abs} = 10\,T_{col}$). The stopping voltage increases with filter height and a higher temperature difference exhibits larger stopping voltage values.

tion of the filter height. The two curves correspond to two different temperature differences: $T_{abs} = 10\,T_{col}, 20\,T_{col}$, which represent two different illumination conditions, which we call cloudy and sunny, respectively. As expected, the plot shows that a higher temperature difference results in a higher stopping voltage. There are indeed more high energy electrons available for extraction. Furthermore, this result demonstrates that a higher filter height induces a higher stopping voltage.
Now, we examine the behavior of μ as a function of time in two different illumination conditions. Figure 4.3. depicts the potential buildup, at a fixed filter height (specifically $\epsilon_1 = 10\,T_{col}$) as a function of time. The buildup increases until the stopping voltage is reached at a certain time and remains constant afterwards. However, we observe a noticeable contrast in how fast the stopping voltage is reached depending on the temperature difference. As expected, for a higher temperature difference

(sunny) the stopping voltage is reached faster than for a lower temperature difference (cloudy). Thus, we observe that there's a specific charging time required for

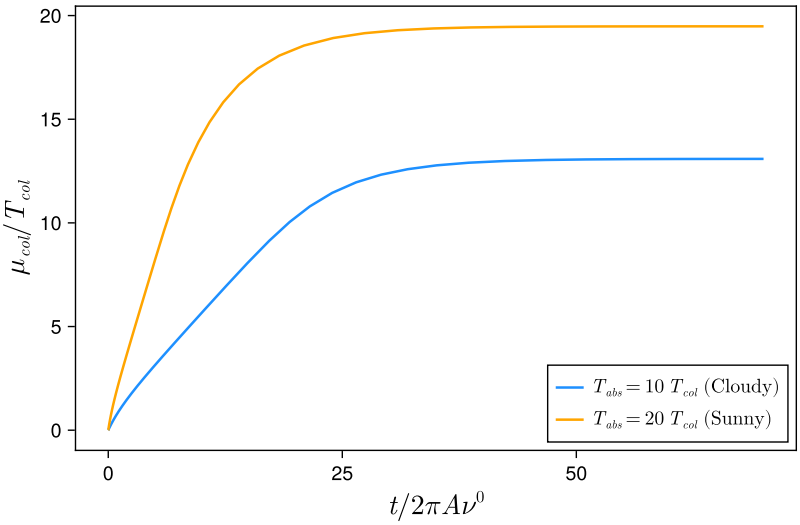

Figure 4.3: Chemical potential as a function of time at fixed $\epsilon_1 = 10\,T_{col}$ for cloudy and sunny illumination conditions. A higher temperature difference induces higher chemical potential as expected and requires less time to reach the stopping voltage.

reaching the stopping voltage and how fast this is reached depends on the temperature difference between the absorber and the collector. For practical reasons, the charging time is limited in reality so we take this physical constraint into account. We will now look into setting a limit on the charging time.

4.2 Potential buildup in a given charging time

Now, we study the potential buildup that can be reached in a given charging time and analyze whether the plateau value (stopping voltage) is reached within this time interval. We start by analyzing the effect of the filter height on the potential buildup under different non-equilibrium conditions. As an example, we set the t_{max} at $500 \times 2\pi A\nu^0$ to find the ideal filter height at this specific charging time. Starting with the no feedback case, different filter heights are tested in both sunny and cloudy illumination conditions.
In Figures 4.4 and 4.5, we show μ as a function of time at $T_{abs} = 10\,T_{col}$ (cloudy). The plateau buildup previously shown in Figure 4.3 is seen here again. We also find that the larger the filter height, the higher the plateau value, namely, higher stopping voltage. Interestingly, we see that the larger the stopping voltage, the later this is reached. For example, for $\epsilon_1 = 40\,T_{col}$, the plateau is not reached within the given charging time ($t_{max} = 500 \times 2\pi A\nu^0$), in the cloudy setup. An important aspect learned from this plot is that there's a tradeoff between charging time and reached stopping voltage.
When increasing the temperature difference, this behavior changes. This is demonstrated in Figure 4.5 showing the same potential buildup as a function of time and at the same filter heights but at a higher temperature difference, at $T_{abs} = 20\,T_{col}$

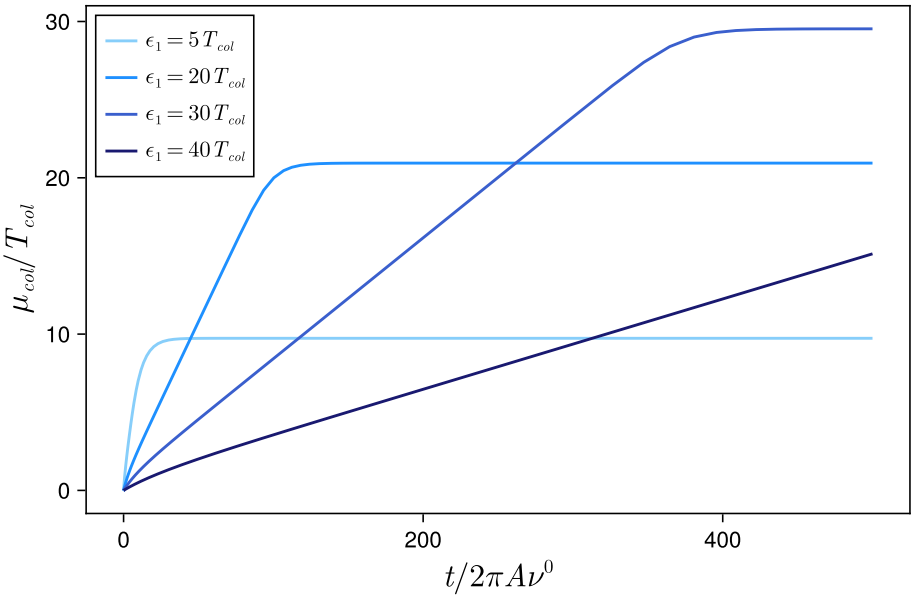

Figure 4.4: Chemical potential over time set at $T_{abs} = 10\,T_{col}$ (cloudy) for four different filter heights. Only the filter height at $40\,T_{col}$ failed to reach the plateau– indicating that it needs more time to reach the stopping voltage. Within this time interval, $30\,T_{col}$ obtained the highest stopping voltage but considerably takes longer to reach the stopping voltage.

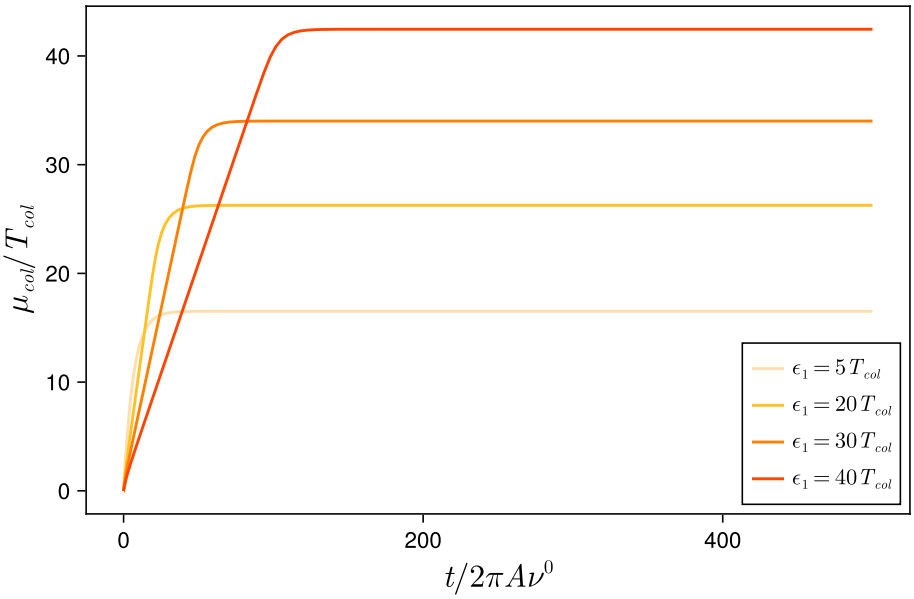

Figure 4.5: Chemical potential over time set at $T_{abs} = 20\,T_{col}$ (sunny) for four different filter heights. Due to the high temperature difference, more high energy electrons are extracted. Hence, all filter heights tested reached their respective stopping voltage within this time interval. The highest filter height $40\,T_{col}$ obtained the highest stopping voltage but takes slightly longer to reach the stopping voltage.

(sunny). The first important thing to note is that the reached stopping voltage is significantly higher than in the small temperature difference regime. Moreover, for all filter heights, the stopping voltage is reached within the charging time. Note that the difference between the charging time among the various filter heights is very little in this high temperature difference regime relative to the low temperature difference regime. Furthermore, the comparison of these two figures demonstrates the expected better performance that can be reached in the sunny case. Importantly, we also find that within a fixed charging time, a lower filter height is convenient for the cloudy situation while a higher filter height would be more convenient for the sunny condition. This motivates the next step, namely, to implement a feedback that, for a given charging time, modifies the filter height depending on the non-equilibrium potential conditions.

4.3 Improved battery charging using the feedback

Incorporating the feedback mechanism in our calculations we find the following time-dependent chemical potential:

$$\begin{aligned}\frac{d\mu}{dt} = \frac{1}{2\pi\nu^0}\left[1+\exp\left(-\frac{\mu(t)}{T_{col}}\right)\right] \\ \times\left\{T_{abs}\ln\left[1+\exp\left(-\frac{\epsilon_1-\mathrm{U}f_{col}(\epsilon_{dot}).}{T_{abs}}\right)\right]\right. \\ \left.-T_{col}\ln\left[1+\exp\left(\frac{\mu(t)-\epsilon_1-\mathrm{U}f_{col}(\epsilon_{dot}).}{T_{col}}\right)\right]\right\}\end{aligned} \tag{4.8}$$

where U is the coupling parameter and ϵ_{dot} is the energy level of the quantum dot. Similar to the no feedback setup, Eq. (4.8) is solved computationally using *DifferentialEquations.jl* in Julia [30].

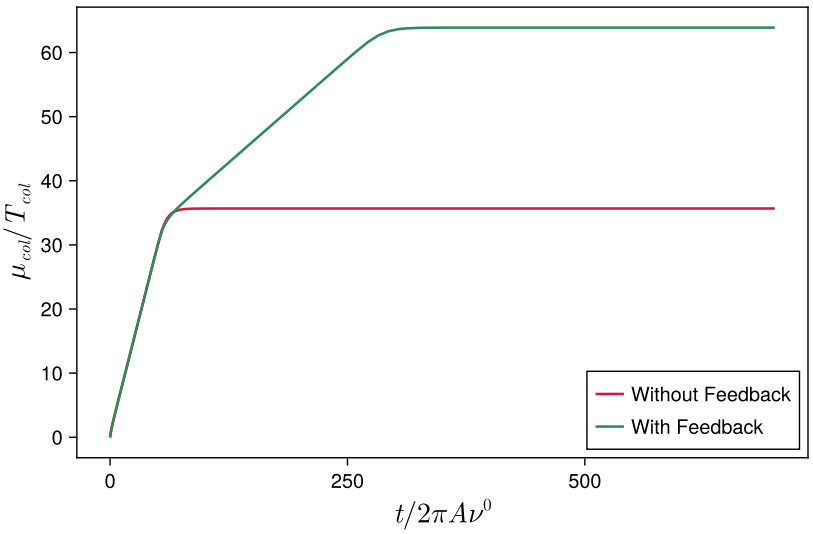

Figure 4.6: Chemical potential buildup as a function of time, with and without feedback.

A comparison of the time evolution of the chemical potential with and without feedback is shown in Fig. 4.6 where the chemical potential is plotted as a function of time, both with feedback and without. The values used for the feedback parameter are: $\epsilon_1 = 32.03\,T_{col}, \epsilon_{dot} = 33.31\,T_{col}$, and U $= 31.63\,T_{col}$ (and are obtained in Section 4.4). The same values for ϵ_1 and at the same $T_{abs} = 20\,T_{col}$ were used to obtain the curve without feedback. When feedback is used, the chemical potential does not plateau at the stopping voltage observed without feedback. Instead, the chemical potential continues to increase, reaching a higher stopping voltage. This is due to the feedback responding to the increase in μ_col and how this increase eventually leads to the quantum dot being occupied, thereby lifting the filter height by U. This mechanism happens at the point where the slope of curve changed. Due to this change in slope, there are now two distinct charging times in the feedback case. The potential buildup initially exhibits a steep slope similar to what would happen without feedback. Then, at the point where the no-feedback case would plateau, it shifts to a gentler slope before reaching the stopping voltage. This overall trend explains how the feedback makes the system reach the stopping voltage faster as compared to a simple linear increase from zero to the same stopping voltage.

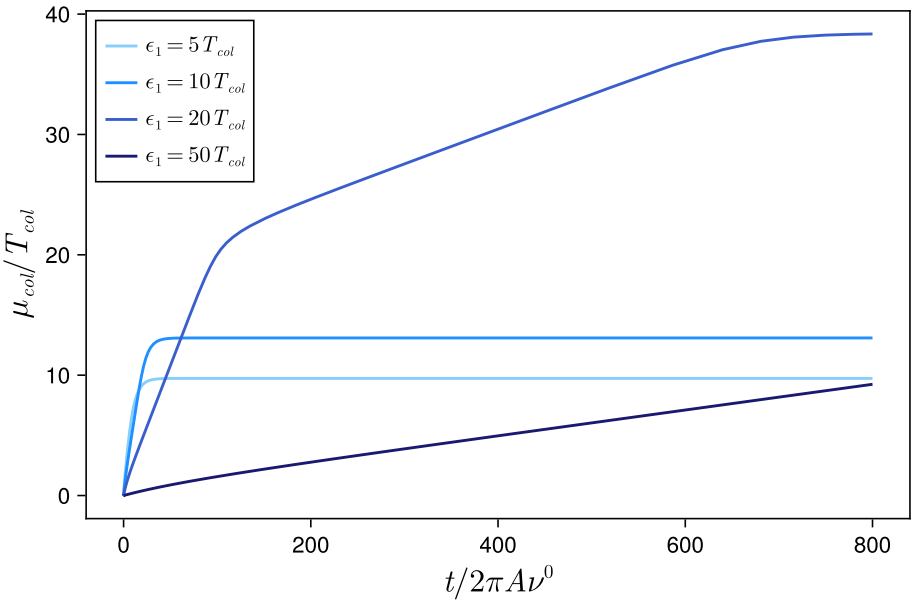

Figure 4.7: Chemical potential as a function of time for four different filter heights at $T_{abs} = 10\,T_{col}$. The sharp transitions in slope featured in the filter height at $20\,T_{col}$ indicates the impact of the feedback. Moreover, due to the lower temperature difference, the highest filter height $50\,T_{col}$ did not have enough time to plateau.

We now study how the feedback setup behaves for different starting filter heights and under different illuminations. Figure 4.7 shows the chemical potential as a function of time when feedback is active, for different filter heights ϵ_1 and in cloudy conditions. We observe a sharp transitions in slope in the case where $\epsilon_1 = 20\,T_{col}$. This indicates the impact of the feedback. Moreover, due to the low temperature difference, in the case of a highest filter height $50\,T_{col}$, the chemical potential did not plateau in the given time. For lower filter heights, the chemical potential required to activate the feedback was not reached, hence no change of slopes are observed.

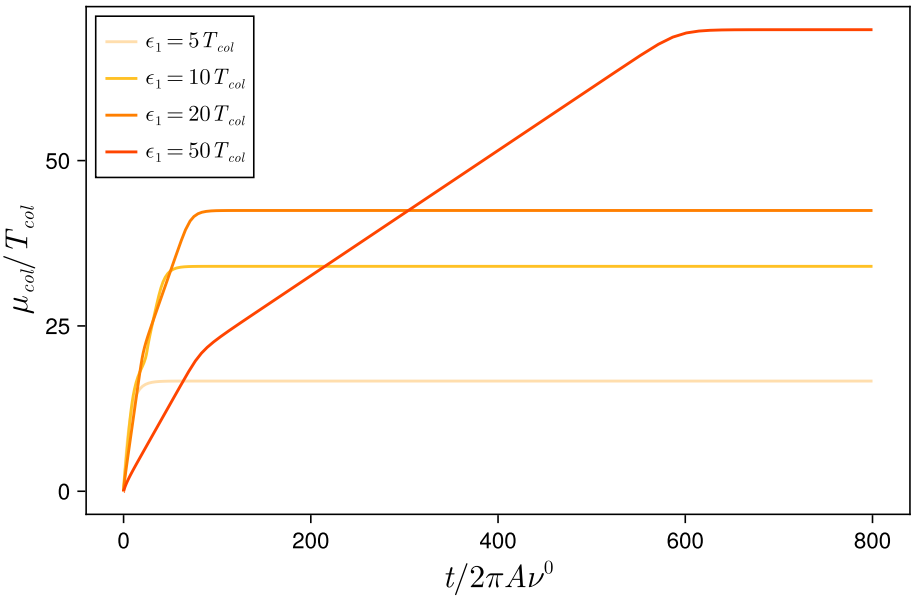

Figure 4.8: Chemical potential as a function of time for four different filter heights at $T_{abs} = 20\,T_{col}$. The same sharp transitions in slope are observed here. The highest filter height $50\,T_{col}$ managed to plateau at a significantly higher stopping voltage due to the higher temperature difference.

Figure 4.8 shows the chemical potential as a function of time when feedback is active, for different filter heights ϵ_1 and in sunny conditions. The same sharp transitions in slope as in the cloudy case are observed here. In the case of large filter height $50\,T_{col}$, the given time is enough for the chemical potential to plateau. This happens for a significantly higher stopping voltage than in the cloudy case due to the higher temperature difference. The cases of other filter heights also show changes of slope, except for the lowest one, for the same reason as in the cloudy case.
Thus, similarly to the case without feedback, we consistently see that the appropriate filter height depends on the required time to reach the stopping voltage within the given t_{max}, and on the influence of T_{abs} on how fast this is reached. A method to build an optimized hot carrier solar cell based on the t_{max} and temperature difference is provided in the next section.

4.4 Building an optimized hot carrier solar cell

In this section, we consider the potential buildup reached in a given time t_{max}, and try to find the optimal parameters ($\epsilon_1, \epsilon_{dot}$, and U) that maximize it. In the previous chapter (about powering an electric device with the cell), the ideal filter heights corresponding to each illumination condition (sunny and cloudy) were obtained to acquire the proper corresponding values for U and ϵ_{dot}. We apply a similar method here to obtain these parameters but in the context of optimizing the charge buildup in the battery.
Figure 4.10 shows the flow chart depicting each step taken to obtain these optimal parameters given a t_{max} and two temperature differences. We proceed as follows.

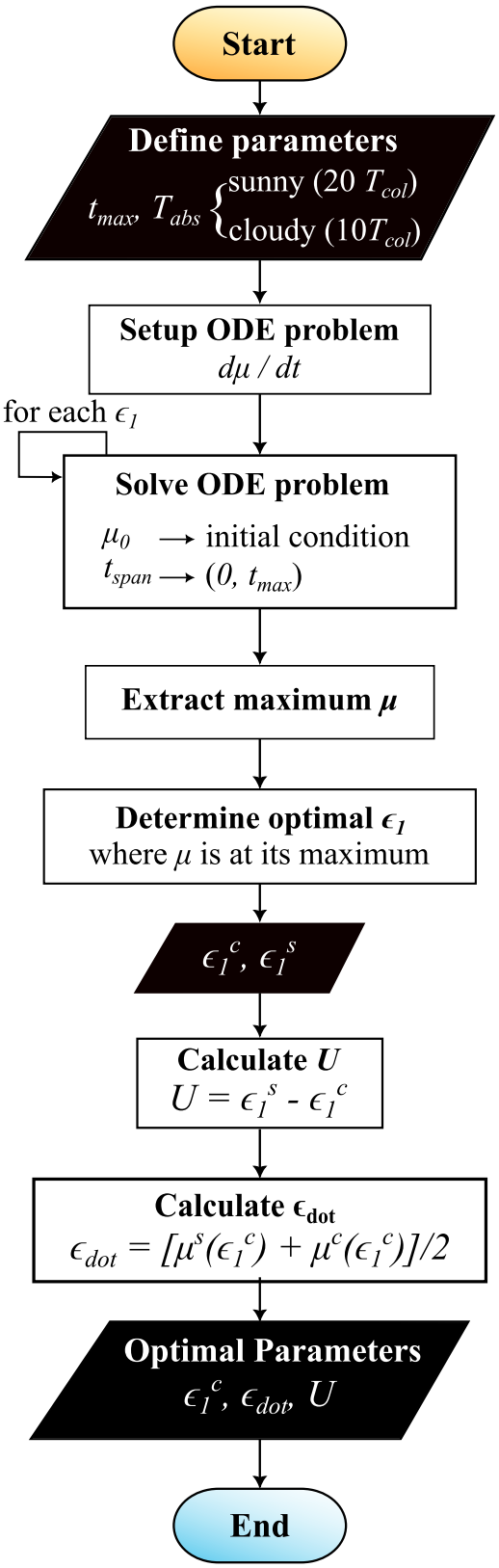

Figure 4.9: Flow chart of building an optimized hot carrier solar cell for charging a battery.

Firstly, the input parameters are given. In this scenario, we set $t_{max} = 500 \times 2\pi A\nu^0$ and, as used throughout this thesis, $T_{abs} = 10\,T_{col}$ and $20\,T_{col}$ are the temperature values set for cloudy and sunny illumination conditions, respectively. Eq. (4.8) is then set up using these input parameters as an ordinary differential equation problem. As previously mentioned, we use the *DifferentialEquations.jl* to solve this problem for μ_{col} in the time interval $t_{span} \in [0; t_{max}]$. This is repeated for various values of $\epsilon_1 \in [0; 200\,T_{col}$, therefore yielding a time series of $\mu(t)$ for each value of ϵ_1. Afterwards, we extract the maximum μ_{col} from each ϵ_1. This process is performed for both illumination condition. We then pick the highest chemical potential and the corresponding filter height at which it was reached. These filters heights, for cloudy and sunny illumination conditions, are called ϵ_1^c and ϵ_1^s, respectively. As was done in the previous chapter the coupling parameter is calculated according to Eq. (3.11).

$$U = \epsilon_1^s - \epsilon_1^c \tag{4.9}$$

and this corresponds to the desired change in height as we shift from cloudy to sunny condition. Similarly, the ϵ_{dot} is obtained from Eq. (3.12)

$$\epsilon_{dot} = \frac{\mu_{col}^s(\epsilon_1^c) + \mu_{col}^c(\epsilon_1^c)}{2}. \tag{4.10}$$

Here, in the same manner as computed in the previous chapter, the chemical potentials, both reached at the ideal filter height for the cloudy condition ϵ_1^c are needed to provide the optimal energy level of the quantum dot. Here, the μ_{col}^c is the maximum chemical potential in the cloudy condition and the μ_{col}^s is the potential in the sunny condition when the filter height is at ϵ_1^c. The initial filter height should be ϵ_1^c, otherwise, the feedback mechanism would not be activated in time. If the solar cell has an initial filter height ϵ_1^c, then a sunny or a cloudy condition would allow the feedback to respond quickly to any nonequilibrium conditions brought upon by changes in the temperature difference. However, when starting from a higher filter height ϵ_1^s and initially exposed to a cloudy condition, the filter height would be too high–effectively blocking most of the low energy electrons from the absorber. It would take a longer time to charge the battery.

Now that we have established the process to build an optimized hot carrier solar cell, the optimal parameters obtained will be used to model the chemical potential as a function of time. At $t_{max} = 500 \times 2\pi A\nu^0$, the optimal parameters acquired are as follows: $\epsilon_1 = 32.03\,T_{col}$, $\epsilon_{dot} = 33.31\,T_{col}$, and U $= 31.63\,T_{col}$. The resulting chemical potential from using the optimal parameters are then compared to non-optimal parameters. These non-optimal parameters are simply taken from the optimal parameters but offset ϵ_1 by $\pm 15 T_{col}$.

We plot the chemical potential as a function of time to show how the optimized solar cell performs versus the non-optimized ones in Figure 4.10. We observe the sharp transitions in slope as featured previously in section 4.3 in all the potentials presented. All potentials reached the stopping voltage but the time it took them to do so vary. Specifically, at $t_{max} = 500 \times 2\pi A\nu^0$, the optimized potential achieved the highest stopping voltage at a later time compared to the non-optimized (lower bound) potential and sooner than the non-optimized (upper bound) potential. However, looking at earlier times, there's a moment where the non-optimized (lower bound)

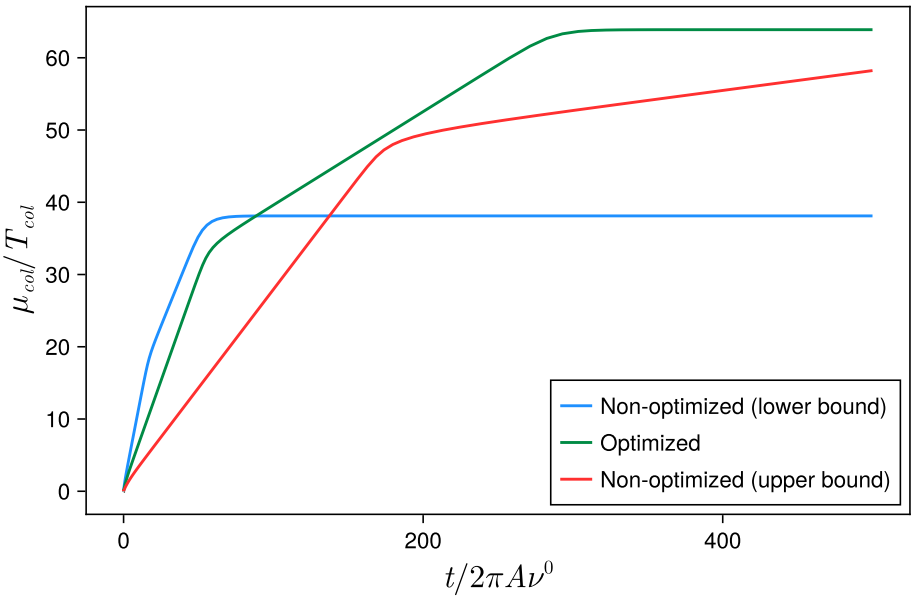

Figure 4.10: Chemical potential plotted as a function of time using parameters ($\epsilon_1, \epsilon_{dot}$, and U) obtained from the discussed method of building an optimized hot carrier solar cell (green) compared to non-optimized parameters, which are taken by offsetting the optimized ϵ_1 by ± 15 (blue for lower bound and red for upper bound).

potential is higher than the optimized one. Nevertheless, as soon as it plateaus, the optimized potential takes over to reach a higher stopping voltage. Meanwhile, the non-optimized (upper bound) parameters consistently induced lower potential across t_{span} and never reached the stopping voltage. Overall, in the given t_{max}, the optimized parameters have proven to be appropriate in this specific scenario.
Unfortunately, in terms of the accuracy of the provided method, we encountered a problem. First of all, despite being optimized at $t_{max} = 500 \times 2\pi A\nu^0$, the optimized potential reached the stopping voltage before this time, specifically around $300 \times 2\pi A\nu^0$. This shows that the method did not give proper optimal parameters so that the the highest stopping voltage, right before the plateau, is reached specifically at the given t_{max}. Indeed, our method does not take into account the fact that there is a change of slope when the feedback becomes active. Hence, further research is needed to update the method in order to improve its accuracy. Here, we have focused on feedback that can increase the stopping voltage within the given charging time, by measuring the chemical potential in the collector. In the future, it would be promising to implement a similar feedback mechanism that relies on the measurement of the temperature difference between the two contacts.

5

Conclusion

5.1 Summary

In this thesis, opportunities for improving the performance of a hot-carrier solar cells using feedback were studied. Hot-carrier solar cells have been proposed to exploit the excess energy of created electron-hole pairs, which is lost in standard solar cells due to thermalization before the charge carriers get extracted. The working principle of a hot-carrier solar cell exploits energy filtering, such that a higher voltage build-up is allowed without a backflow from the collector back into the absorber. This energy filtering clearly leads to a trade-off between the value of the generated potential difference and the value of the induced current flowing through the load, since low-energy carriers are filtered out and hence not used.

In this project, we have first analyzed the “basic" operation of such hot-carrier solar cells for different operation conditions and different implementations for energy-filtering. Importantly, we have studied both the situation where the solar cell is used to charge a battery (open circuit configuration) and where power is generated by inducing a current through a load (closed circuit configuration). The theoretical tool used for our analysis is scattering theory and we have furthermore used *NonlinearSolve* and *DifferentialEquations* packages in Julia to numerically optimize the operation.

The tradeoff between high current generation and high voltage buildup is where our feedback idea sets in. In order to improve the basic performance, we have proposed to use a quantum dot “measuring” the voltage buildup in the collector and modifying the energy-filtering properties via capacitive coupling to the filter connecting absorber and collector. While the feedback we have analyzed here is based on measurement of the potential that is built up in the collector either due to charging for the battery setup or due to the potential drop at the load under steady-state operation, it thereby also contains the effect of modified illumination conditions of the solar cell, because this directly impacts the build-up of the potential.

In this report, we have shown in detail the working principle of this feedback mechanism and have explicitly shown under which conditions and to which extent it improves the solar cell’s performance. We have shown how feedback can significantly improve the performance both for improved adaptability in the closed circuit with a load and for an improved charging time of the battery.

5.2 Outlook

Although we have demonstrated the importance of feedback on improving the performance of a hot carrier solar cell, there are still certain aspects that need further development. In chapter 3, we successfully showed how the feedback adapts to two particular temperature settings. However, a feedback mechanism that flexibly adjust to continuous temperature changes is still to be developed. We therefore plan for a more general numerical optimization for the feedback mechanism under steady state operation.
In chapter 4, we aimed for obtaining the highest stopping voltage within a certain charging time by using the optimal parameters acquired with the simple method proposed in Chapter 3. The method may have been too simple as the resulting parameters did not lead to the highest stopping voltage possible specifically at the maximum charging time. Hence, the proposed method needs to be more sophisticated to return parameters that will fully optimize the solar cell.
Throughout we have only considered an ideal measurement. In the future it would be necessary to test how these parameters can be reached in experiments and how deviation from the ideal measurement would impact performance.
Up to now, the feedback, relies on the measurement of the collector contact. Another possible strategy would be to directly measure the temperature of the absorber and employ feedback accordingly. This could be even combined with the feedback studied in this project and realized by doing measurement and feedback with different quantum dots–both coupled to the QPC that give feedback both depending on the created voltage difference and on the applied temperature difference.
Since energy-dependent transmissions in solar cells have been realized, and feedback by capacitively coupled quantum dots is experimentally feasible, we believe that the proposed scheme could be implemented in the near future. It would therefore be important to test our scheme with parameter regimes representing possible future implementations.

Bibliography

[1] L. Tesser, "Fluctuations and nonequilibrium thermodynamics in electronic nanosystems," licentiate thesis, Chalmers University of Technology, Gothenburg, Sweden, 2022.

[2] A. Mohammad Bagher, "Types of Solar Cells and Application," *American Journal of Optics and Photonics*, vol. 3, no. 5, p. 94, 2015.

[3] M. Shahabuddin, M. Asim, and A. Sarwar, "Evolution and Modeling of Solar Photovoltaic Cells: From Early to Modern Concepts," in *Photovoltaic Systems Technology* (M. A. Husain, M. W. Ahmad, F. I. Bakhsh, P. Sanjeevikumar, and H. Malik, eds.), pp. 27–41, Wiley, 1 ed., July 2024.

[4] R. A. Marques Lameirinhas, J. P. N. Torres, and J. P. De Melo Cunha, "A Photovoltaic Technology Review: History, Fundamentals and Applications," *Energies*, vol. 15, p. 1823, Mar. 2022.

[5] J. Nelson, *The Physics of Solar Cells*. Published by Imperial College Press and Distributed by World Scientific Publishing Co., May 2003.

[6] L. Tesser, R. S. Whitney, and J. Splettstoesser, "Thermodynamic Performance of Hot-Carrier Solar Cells: A Quantum Transport Model," *Physical Review Applied*, vol. 19, p. 044038, Apr. 2023.

[7] R. T. Ross and A. J. Nozik, "Efficiency of hot-carrier solar energy converters," *Journal of Applied Physics*, vol. 53, pp. 3813–3818, May 1982.

[8] A. P. Kirk and M. V. Fischetti, "Fundamental limitations of hot-carrier solar cells," *Physical Review B*, vol. 86, p. 165206, Oct. 2012.

[9] S. Kahmann and M. A. Loi, "Hot carrier solar cells and the potential of perovskites for breaking the Shockley–Queisser limit," *Journal of Materials Chemistry C*, vol. 7, no. 9, pp. 2471–2486, 2019.

[10] D. K. Ferry, S. M. Goodnick, V. R. Whiteside, and I. R. Sellers, "Challenges, myths, and opportunities in hot carrier solar cells," *Journal of Applied Physics*, vol. 128, p. 220903, Dec. 2020.

[11] I. Konovalov and V. Emelianov, "Hot carrier solar cell as thermoelectric device," *Energy Science & Engineering*, vol. 5, pp. 113–122, June 2017.

[12] F. Michelini, A. Crépieux, F. Gibelli, J.-F. Guillemoles, N. Cavassilas, and R. Whitney, "How does energy filtering improve quantum-dot based photovoltaic devices," in *Communication Dans Un Congrès*, 2015. Presented at a conference, archived on HAL.

[13] G. Conibeer, R. Patterson, P. Aliberti, L. Huang, J.-F. Guillemoles, D. König, S. Shrestha, R. Clady, M. Tayebjee, T. Schmidt, and M. Green, "Hot carrier solar cell absorbers," in *Proceedings of the 24th European Photovoltaic Solar*

Energy Conference, (Hamburg, Germany), pp. 37–42, WIP Renewable Energies, 2009.

[14] D. König, K. Casalenuovo, Y. Takeda, G. Conibeer, J. Guillemoles, R. Patterson, L. Huang, and M. Green, "Hot carrier solar cells: Principles, materials and design," *Physica E: Low-dimensional Systems and Nanostructures*, vol. 42, pp. 2862–2866, Sept. 2010.

[15] B. Bertin-Johannet, T. Thuégaz, J. Splettstoesser, and R. S. Whitney, "Improving photovoltaics by adding extra terminals to extract hot carriers," 2025. Version Number: 1.

[16] R. Landauer, "Electrical resistance of disordered one-dimensional lattices," *Philosophical Magazine*, vol. 21, pp. 863–867, Apr. 1970.

[17] M. Büttiker, Y. Imry, R. Landauer, and S. Pinhas, "Generalized many-channel conductance formula with application to small rings," *Physical Review B*, vol. 31, pp. 6207–6215, May 1985.

[18] E. V. Sukhorukov, "Scattering theory approach to bosonization of non-equilibrium mesoscopic systems," *Physica E: Low-dimensional Systems and Nanostructures*, vol. 77, pp. 191–198, Mar. 2016.

[19] G. Hackenbroich, "Phase coherent transmission through interacting mesoscopic systems," *Physics Reports*, vol. 343, pp. 463–538, Mar. 2001.

[20] H. V. Houten, L. W. Molenkamp, C. W. J. Beenakker, and C. T. Foxon, "Thermo-electric properties of quantum point contacts," *Semiconductor Science and Technology*, vol. 7, pp. B215–B221, Mar. 1992.

[21] S. Kheradsoud, N. Dashti, M. Misiorny, P. Potts, J. Splettstoesser, and P. Samuelsson, "Power, Efficiency and Fluctuations in a Quantum Point Contact as Steady-State Thermoelectric Heat Engine," *Entropy*, vol. 21, p. 777, Aug. 2019.

[22] H. Van Houten and C. Beenakker, "Quantum Point Contacts," *Physics Today*, vol. 49, pp. 22–27, July 1996.

[23] J. Fast, Y.-P. Liu, Y. Chen, L. Samuelson, A. M. Burke, H. Linke, and A. Mikkelsen, "Optical-Beam-Induced Current in InAs/InP Nanowires for Hot-Carrier Photovoltaics," *ACS Applied Energy Materials*, vol. 5, pp. 7728–7734, June 2022.

[24] J. Fast, H. Lundström, S. Dorsch, L. Samuelson, A. Burke, P. Samuelsson, and H. Linke, "Geometric Symmetry Breaking and Nonlinearity Can Increase Thermoelectric Power," *Physical Review Letters*, vol. 133, p. 116302, Sept. 2024.

[25] J. Yang, C. Elouard, J. Splettstoesser, B. Sothmann, R. Sánchez, and A. N. Jordan, "Thermal transistor and thermometer based on Coulomb-coupled conductors," *Physical Review B*, vol. 100, p. 045418, July 2019.

[26] A. Pal, F. Holtorf, A. Larsson, T. Loman, F. Schaefer, Q. Qu, A. Edelman, and C. Rackauckas, "Nonlinearsolve. jl: High-performance and robust solvers for systems of nonlinear equations in julia," *arXiv preprint arXiv:2403.16341*, 2024.

[27] R. S. Whitney, "Finding the quantum thermoelectric with maximal efficiency and minimal entropy production at given power output," *Physical Review B*, vol. 91, p. 115425, Mar. 2015.

[28] M. Büttiker, H. Thomas, and A. Prêtre, "Mesoscopic capacitors," *Physics Letters A*, vol. 180, pp. 364–369, Sept. 1993.

[29] J. Gabelli, G. Fève, J.-M. Berroir, B. Plaçais, A. Cavanna, B. Etienne, Y. Jin, and D. C. Glattli, "Violation of Kirchhoff's Laws for a Coherent *RC* Circuit," *Science*, vol. 313, pp. 499–502, July 2006.

[30] C. Rackauckas and Q. Nie, "DifferentialEquations.jl–a performant and feature-rich ecosystem for solving differential equations in Julia," *Journal of Open Research Software*, vol. 5, no. 1, 2017.

DEPARTMENT OF MICROTECHNOLOGY AND NANOSCIENCE (MC2)
CHALMERS UNIVERSITY OF TECHNOLOGY
Gothenburg, Sweden
www.chalmers.se

CHALMERS
UNIVERSITY OF TECHNOLOGY